Analysis of a Series Resonant Converter Pulsewidth-Modulated or Current-Controlled for Low Switching Loss

KHAI D. T. NGO, MEMBER, IEEE

Abstract—**Pulsewidth modulation (PWM) and current-controlled switching are applied to a full-bridge series resonant converter to regulate the output from no load to full load with low switching loss and with a narrow range of frequency variation. Drive strategies, control law, component stress, and other steady-state functions are analyzed for both switching modes.**

I. Introduction

As THE switching frequency is increased into the megahertz range to improve the power density and performance of switched-mode converters, interest has been shifted from pulsewidth modulation (PWM) to current-programmed and resonant modes of operation. Pulsewidth modulation is used in a majority of converters [7] switched below a few hundred kilohertz because of its simplicity. In a PWM converter, the output is controlled by varying the pulsewidth or duty ratio of the switching waveforms. A current loop can be put around a PWM topology as described in [8] to form a current-mode converter. Current-mode control is gaining popularity because it offers improved performances, such as fast response, inherent current protection, and ease of paralleling. In a current-programmed converter, the output is controlled by a reference current, which is compared to a converter current to determine switching instants.

Resonant conversion [3] is preferred to PWM or current-mode control in applications involving high power and high switching frequency. The switching loss in a resonant converter is low because the switching device is turned on or off at practically zero voltage or current. The sensitivity to parasitic inductance or capacitance is reduced because these parasitics can be a part of the resonant circuit.

In its most widely used configuration, a resonant converter is excited by a bipolar square wave, generated from a dc input by a half-bridge or full-bridge circuit. The switching frequency is then varied to control the output voltage. Frequency control, however, causes many problems as the switching frequency has to be varied over a wide range to accommodate the worst combinations of load and line. For operation below resonance, filter components are large because they have to be designed for the lower frequency range. For operation above resonance, fast electronics are required to maintain control at the upper frequency range. Keeping the switching frequency constant and controlling it by pulsewidth modulation [5] are obvious ways to eliminate the problems associated with frequency variation.

Another problem, found in a series resonant converter, is the loss of control at light load [1]. Pulsewidth modulation solves this problem because as the time during which the source is connected to the converter is reduced to zero, so is the output voltage.

It has been observed by Steigerwald [2] that the efficiency in a parallel resonant converter degrades at light load or high line. This is because the power loss, which results from a constant circulating current at the input, is relatively independent of the line or load. Pulsewidth modulation or some current-controlled switching that reduces the amount of circulating current will improve the partial-load efficiency.

There are many ways to apply PWM or current-controlled switching to a resonant topology. In this paper, a type of PWM and a type of current-controlled switching that alleviate the aforementioned problems while keeping the switching loss low are investigated for a full-bridge series resonant converter. A full-bridge topology, frequently used in high-power applications, provides control flexibility unavailable in a half-bridge or single-ended topology. The switching frequency is restricted to above resonance to realize the advantages pointed out in [2]: no turn-on loss, low turn-off loss by capacitive snubber, low commutation stress on the freewheeling diode, and no loss due to high dv/dt or the discharging of device capacitance.

Pulsewidth modulation is treated in Section II and current-controlled switching in Section III. In each section the switching or control strategy is described first and is followed by an analysis of the resulting mode of operation. Experimental results are compared with analytical ones in Section IV. Essential results are summarized at the end.

Manuscript received March 27, 1987; revised August 24, 1987.

The author is with General Electric Co., Corporate Research and Development, Schenectady, NY 12301.

IEEE Log Number 8717895.

II. PWM in a Full-Bridge Series Resonant Converter

A. PWM Switching Strategy

A full-bridge series resonant converter is shown in Fig. 1. It has four switching devices that make up two double-throw switches. The first switch consists of throws s_{11} and s_{12}; the second one consists of s_{21} and s_{22}. Each throw is shown implemented by a field-effect transistor (FET) having an internal inverse diode. The switches generate a bridge voltage v_T that excites a resonant circuit. The resonant circuit consists of a resonant inductor L_r, a resonant capacitor C_r, a rectifier bridge, a filter capacitor C, and a load resistance R. Isolation is possible, but is not shown for clarity.

There are many ways to pulsewidth-modulate v_T. The one of interest is an ac square wave with variable pulsewidth, as shown in Fig. 2(c). It is generated by driving s_{11} and s_{21} with the waveforms shown in Fig. 2(a) and (b), respectively. These waveforms have 50-percent duty ratios and are phase-shifted by an "on" interval t_1 during which the source voltage V_g is applied to v_T. Both s_{11} and s_{21} (or s_{12} and s_{22}) short out v_T during the "idle" interval from t_1 to t_2.

It has been observed that a commutation between the two throws of a double-throw switch generates low switching loss, switching noise, and diode stress when the current is transferred from the FET of the outgoing throw to the freewheeling diode of the incoming throw. Thus the commutation between s_{21} and s_{22} always has these favorable attributes since these throws always conduct through their FET's just before the commutation, as can be seen from Figs. 1, 2(b), and (d). The commutation between s_{11} and s_{12}, on the other hand, is favorable only if $i_r(T/2) \geq 0$, as can be seen from Figs. 1, 2(a) and (d). A sufficient condition for i_r to be nonnegative at $T/2$ is derived below.

B. Analysis of a PWM Full-Bridge Series Resonant Converter

Although the converter can be switched at any frequency in general, it should be switched close to the resonant frequency to realize the maximum range of voltage gain. Under this constraint, it will be shown that the inductor current is discontinuous under most operating conditions to maintain low switching loss. Therefore, the following analysis focuses on the steady-state behavior of a PWM series resonant converter in discontinuous-conduction mode (dcm). The derivations of the curves relating voltage gain, on time, duty ratio, current stress, switching frequency, and load are intended to be generic and design-oriented.

In the analysis, the commutation time of the switch is assumed to be negligible. The switches and energy-storage elements are assumed to be lossless. The ripple on the output voltage V is assumed to be negligible. Discussion and figures usually refer to circuit variables. For the results to be generic, however, most equations are expressed in terms of normalized variables. The base voltage, impedance, current, frequency, and time are defined in the following order:

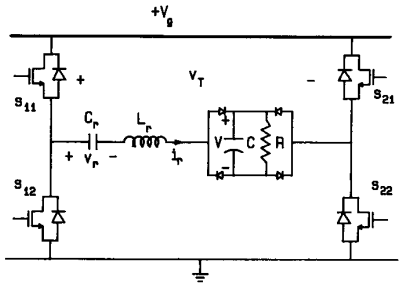

Fig. 1. A full-bridge series resonant converter.

$$V_0 = V_g \qquad R_0 = \sqrt{\frac{L_r}{C_r}} \qquad I_0 = \frac{V_0}{R_0}$$

$$\omega_0 = 2\pi F_0 = \frac{1}{\sqrt{L_r C_r}} \qquad T_0 = \frac{1}{F_0}. \tag{1}$$

The normalized voltage, current, resistance, frequency, and time are defined in the following order:

$$M = \frac{V}{V_0} \qquad J = \frac{I}{I_0} \qquad R_n = \frac{R}{R_0}$$

$$F_n = \frac{F}{F_0} \qquad t_n = \frac{t}{T_0}. \tag{2}$$

If a variable has a subscript (e.g., i_r), its normalized quantity has the same subscript (e.g., j_r).

For dcm to exist two conditions must be met. First i_r must reach zero before half the switching period ends, or the "continuous conduction time" t_2 (see Fig. 2(d)) must satisfy

$$t_2 < \frac{T}{2} \quad \text{or} \quad t_{n2} < \frac{T_n}{2} \tag{3}$$

where T is the switching period, t_{n2} is the normalized t_2, and T_n is the normalized T. Second, to prevent i_r from going negative at t_2, the resonant capacitor voltage V_0 at t_2 (see Fig. 2(e)) should be smaller than output voltage V (see Fig. 1):

$$V_0 < V \quad \text{or} \quad \frac{M_0}{M} < 1 \tag{4}$$

where M_0 is the normalized V_0 and M is the normalized V.

The two preceding equations for dcm can be cast in a more design-oriented form, which includes only the user-controlled switching frequency, on time, and load resistance. To express inequality (4) in this form, observe from Fig. 1 that the load current is the average of the rectified i_r:

$$\frac{V}{R} = \frac{1}{T}\int_0^T |i_r|\, dt. \tag{5}$$

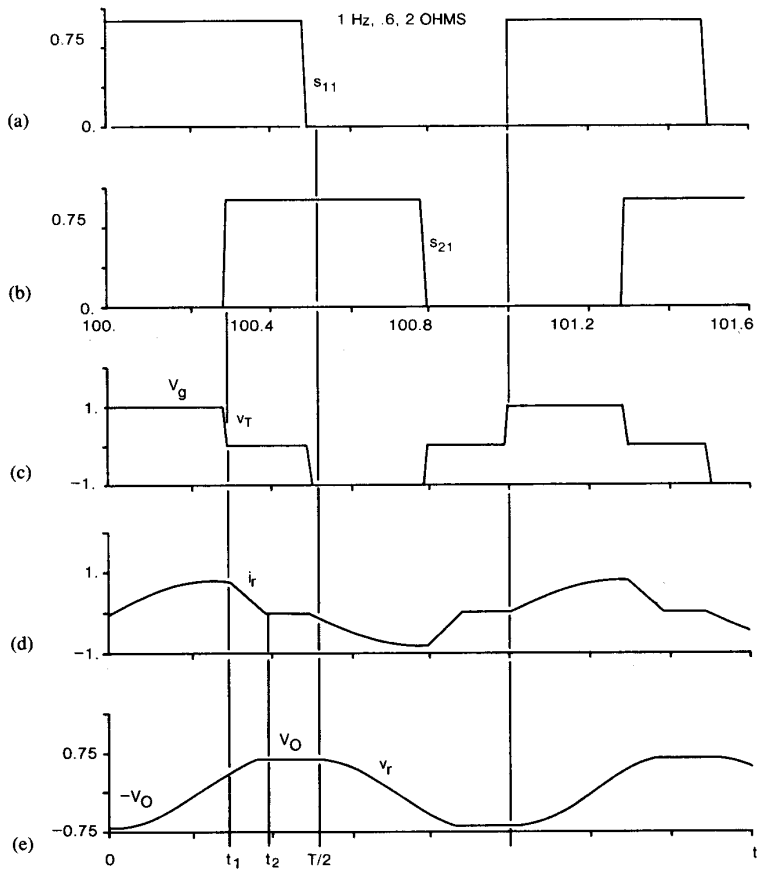

Fig. 2. Phase-shifted drives to s_{11} (a) and s_{21} (b) produce a bipolar square wave with variable pulsewidth (c), which generates the resonant inductor current (d) and resonant capacitor voltage (e).

Since the integral in (5) is proportional to V_0, (5) can be expressed in the following normalized form (see (A13)):

$$\frac{M_0}{M} = \frac{\pi}{2R_nF_n} \tag{6}$$

where R_n is the normalized load resistance and F_n the normalized switching frequency. From (4) and (6), a sufficient condition to prevent i_r from becoming negative at t_2 and to commutate with low loss at $T/2$ is

$$R_nF_n > \frac{\pi}{2}. \tag{7}$$

Thus F_n should be large to drive a small R_n. A larger F_n, however, means a lower peak voltage gain [1] and is undesirable if V needs to be regulated over a wide range of V_g.

A more design-oriented form of inequality (3) would be a curve that relates the on time to the switching period at the boundary of dcm. To obtain this curve, observe that at the dcm boundary,

$$t_{n2} = \frac{T_n}{2} = \frac{1}{2F_n}. \tag{8}$$

Equations (6) and (8) are substituted in (A11) of the Appendix to compute M as a function of T_n for each R_n:

$$M = \frac{1 - \frac{M_0}{M} - \left(1 + \frac{M_0}{M}\right)\cos(2\pi t_{n2})}{1 + \left(\frac{M_0}{M}\right)^2 - \left[1 - \left(\frac{M_0}{M}\right)^2\right]\cos(2\pi t_{n2})}. \tag{9}$$

The resulting M is used to compute t_{n1} given by (A15) of the Appendix:

$$\cos(2\pi t_{n1}) = 1 - \frac{2M}{1 + \frac{2R_nF_n}{\pi}\left(\frac{1}{M} - 1\right)}. \tag{10}$$

The boundary of dcm is then as shown in Fig. 3 for different values of R_n. If an operating point (t_{n1}, T_n) is above the boundary curve, the converter stays in continuous conduction mode with $i_r(T/2) > 0$, a favorable condition in terms of switching loss. If the operating point is below the boundary curve, the mode of operation depends on inequality (7). If this inequality is satisfied, the converter is in dcm. Otherwise, $i_r(T/2) < 0$, causing a lossy

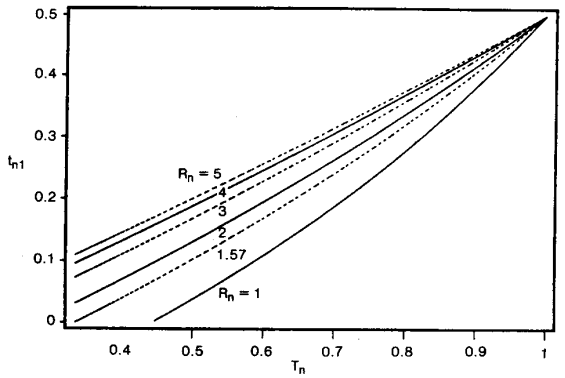

Fig. 3. Normalized on time versus switching period at the boundary of discontinuous conduction mode.

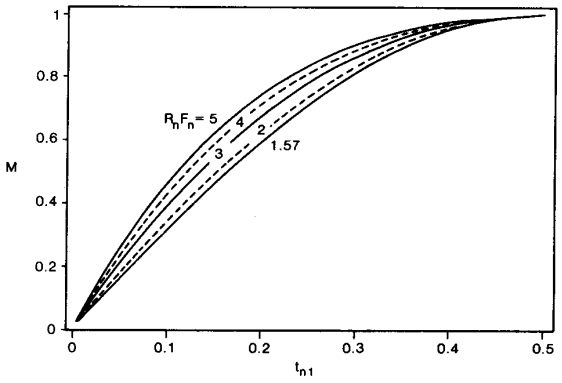

Fig. 4. Voltage gain versus normalized on time for a PWM full-bridge series resonant converter.

and noisy commutation. At $T_n = 1$ (switching at the resonant frequency), t_{n1} at the boundary is at the maximum value of 0.5. Therefore, if the converter is switched at the resonant frequency, it is in dcm for load resistance satisfying inequality (7).

The voltage gain in (10) is plotted against the normalized on time in Fig. 4 for all combinations of R_n and F_n belonging to the dcm regime specified by Fig. 3. It is unity for $t_{n1} = 0.5$, which corresponds to switching at the resonant frequency and using the traditional square-wave drive. It is zero for $t_{n1} = 0$. Thus PWM at the resonant frequency provides the full range of voltage gain of a series resonant converter.

If the switching frequency is known, it is customary to define as control quantity the duty ratio

$$D = 2\frac{t_{n1}}{T_n} = 2t_{n1}F_n. \tag{11}$$

Two sets of curves relating voltage gain to duty ratio are plotted in Fig. 5 for different values of R_n. The curves for $F_n = 1$ are essentially the same as those in Fig. 4. Those for $F_n = 2$ terminate at the boundary at dcm. The completion of these curves is a goal for future research.

A relationship between t_{n2} and t_{n1} is derived by substitution of (9) into (10) and use of (6). The result is plotted in Fig. 6. It is useful in calculation of component ratings.

Another useful curve is that of switch current stress versus voltage gain. To derive this curve, (10) is used to compute t_{n1} as a function of M. If $t_{n1} < 1/4$, it is substituted in (A4) to find the normalized peak switch current J_p; otherwise, $t_{n1} = 1/4$ is used in (A4) to find J_p. Thus

$$J_p = 1 - \left(1 - \frac{\pi}{2R_nF_n}\right)M, \qquad t_{n1} \geq \frac{1}{4} \tag{12a}$$

$$J_p = \left[1 - \left(1 - \frac{\pi}{2R_nF_n}\right)M\right]\sin(2\pi t_{n1}), \qquad t_{n1} < \frac{1}{4}. \tag{12b}$$

The above equations are plotted in Fig. 7. For high M or t_{n1}, (12a) applies and J_p decreases with M. For low M or t_{n1}, (12b) applies and J_p increases with M since $\sin(2\pi t_{n1})$

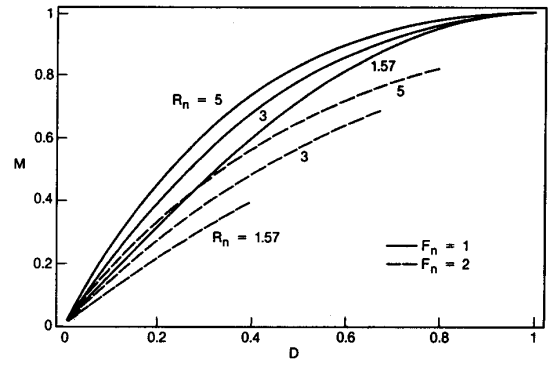

Fig. 5. Voltage gain versus duty ratio.

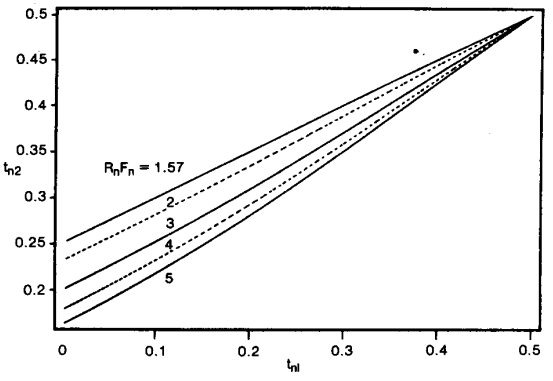

Fig. 6. Normalized continuous conduction time versus normalized on time.

dominates the product. The peaking behavior of the curves in Fig. 7 is strongly related to the improvement of the form factor of i_r at high M or t_{n1}. As the form factor is improved, a lower peak switch current is needed for the same output current. Therefore, a converter should be designed to stay in the high-gain regime as much as possible, where the "high-gain regime" is the range of voltage gain over which J_p decreases with increasing M. The switching device should be selected to carry the maximum peak current encountered. It can be seen from Fig. 7 that

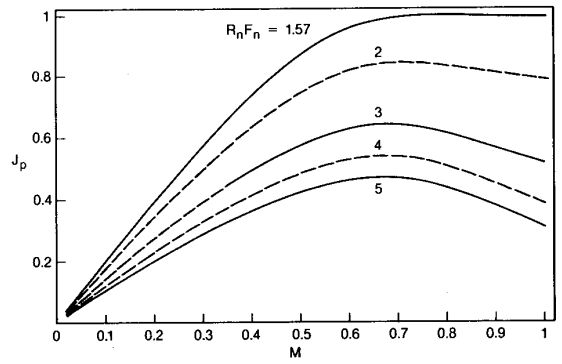

Fig. 7. Normalized peak switch current versus voltage gain for PWM operation.

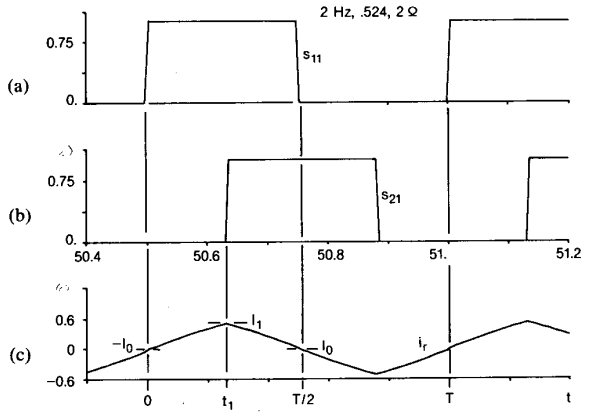

Fig. 8. In current-controlled switching, s_{11} (a) is turned on when i_r (c) crosses $-I_0$; s_{21} (b) is turned on at t_1 when $i_r = I_1$.

this value occurs when the input voltage is highest (or M is lowest in the high-gain regime) and when the load resistance is lowest.

From a design viewpoint, a non-normalized form of (12) is more helpful. It can be reconstructed from (1), (2), and (12a):

$$I_p = \frac{V_g - V}{R_0} + \frac{\pi V}{2RF_n} \tag{13}$$

where I_p is peak switch current. The above equation suggests that over the high-gain region, the current stress should be specified for the maximum V_g and minimum R (note that the same conclusion was reached in the previous paragraph). The resonant characteristic resistance R_0 should be large to bring device current stress down. However, a compromise needs to be made with (6) or (7), which calls for a small R_0 to reduce the voltage stress on C_r and to drive a heavy load with low switching loss.

In summary, with PWM the switching frequency need not be varied to control a series resonant converter. Switching loss and noise are low in a properly designed converter, which usually stays in discontinuous conduction mode. The PWM method described, however, does not favor an extremely heavy load (e.g., short circuit), which necessitates a trade-off between switch current stress and switching loss.

III. Current-Controlled Switching in a Full-Bridge Series Resonant Converter

A. Current-Controlled Switching Strategy

One objective of current-controlled switching is to switch at very low loss over all values of load. The second objective is to minimize the amount of circulating current, or current flowing back to the source through the freewheeling diodes. The third objective is to eliminate dcm, which causes poor form factor and problems associated with high dv/dt. The switching frequency is allowed to vary to achieve these objectives. Hopefully, the range of frequency variation is still much narrower than that needed in the traditional square-wave drive.

The above goals are realized by using the inductor current (whose segments are with the switch currents) to determine the switching points. The switching strategy is explained in Fig. 8. When i_r (Fig. 8(c)) crosses $-I_0$, s_{11} (Fig. 8(a)) is turned on to initiate the "on" interval. (It is important to note that I_0 is shown to be zero just for simplicity. To reduce switching loss and stress, it is preferable to have $I_0 > 0$ so that the commutation occurs before i_r crosses zero.) After s_{11} has been on, a control law can be used to determine when to activate s_{21} to terminate the on interval and to start the "idle" period. This control law can be a simple on-time control or can be more sophisticated implementations of current programming, as described in [6]. For simplicity, s_{21} is shown to be turned on after a duration t_1 has elapsed (on-time control) or when i_r has reached a reference value I_1 (simplistic current programming). When i_r crosses I_0 at the end of the first half cycle, s_{12} is turned on to start another on/idle sequence

As noted above, the commutation experiences low loss and noise when it occurs before i_r crosses zero. This is because it involves turning off an active device and turning on a freewheeling diode and allows lossless capacitive snubbing. Discontinuous conduction is obviously avoided since i_r has neither a chance to reach zero nor enough time to remain at zero. The amount of power returned to the source can be reduced to zero by reducing I_0 (see Fig. 8(c)) to zero. Reducing I_0 also helps to reduce turn-off loss. However, I_0 should be large enough so that the voltage across the incoming FET has a chance to discharge to zero before this FET is actively turned on by its gate drive.

To summarize, current-controlled switching certainly fulfills all the objectives set forth earlier. The switching frequency, however, is no longer constant. The extent to which the switching frequency has to change to supply the entire range of voltage gain is discussed next.

B. Analysis of Current-Controlled Switching Operation

The following analysis is for the current-controlled switching in which the on interval starts at the instant i_r crosses zero, as shown in Fig. 8. It can be seen that the waveforms in Fig. 8 are the same as those of a PWM

series resonant converter with $t_2 = T/2$. Therefore, the relevant equations presented in the previous section apply provided (8) is used for t_{n2}.

The relationship between voltage gain and normalized switching frequency needs to be checked first. It is derived by substitution of (6) and (8) into (9):

$$M = \frac{1 - \frac{\pi}{2R_nF_n} - \left(1 + \frac{\pi}{2R_nF_n}\right)\cos\left(\frac{\pi}{F_n}\right)}{1 + \left(\frac{\pi}{2R_nF_n}\right)^2 - \left[1 - \left(\frac{\pi}{2R_nF_n}\right)^2\right]\cos\left(\frac{\pi}{F_n}\right)}. \quad (14)$$

The range over which F_n needs to vary to realize the full range of M is plotted in Fig. 9 for some values of R_n. A comparison of this plot with a similar one in [1] reveals that F_n of current-controlled switching varies over a much narrower range than F_n of the conventional square-wave drive. For instance, F_n is only 1.08 in Fig. 9 while it has to be 1.21 in the square-wave drive for $M = 0.2$ and $R_n = 0.1$.

To understand why F_n in current-controlled switching varies over a narrow range to achieve line or load regulation, consider the linear circuit in Fig. 10, which models the fundamental components of the ac waveforms in Fig. 1. The effective load seen at the input of the rectifier bridge is represented by the resistance R'. The series combination of R' and the LC tank is driven by v_T', where a prime (') denotes the fundamental component of an exact waveform, v_T in this case. Suppose now that the load is constant while the line is disturbed, and that the switching frequency is varied to regulate the output voltage. Constant R' and V' mean that the output power and, hence, input power, are constant. To keep the input power constant while v_T' fluctuates, the impedance seen by v_T' must change. This impedance change necessitates a change in F_n.

In a straightforward square-wave drive, a large change in V_g causes a proportionally large change in v_T'. Therefore, F_n varies by a fair amount to keep the output regulated. In the drive delineated in Fig. 8, switching at $i_r = 0$ and idling after t_1 effectively "pre-regulate" v_T' such that v_T' does not vary as much as V_g. Therefore, F_n varies by just a small amount to keep the output voltage constant. There is probably an optimal profile of I_0 that minimizes the change in F_n while maintaining low switching loss.

Recall that one of the problems with a square-wave drive is the loss of control at light load. Current-controlled switching only partially solves this problem. It can be inferred from Fig. 9 that for R_n greater than unity, F_n has to change by a factor greater than two to produce the whole range of voltage gain. If such a change is undesirable, it can be avoided by clamping the switching frequency to some maximum value and applying PWM to bring the output voltage to zero. Thus frequency variation

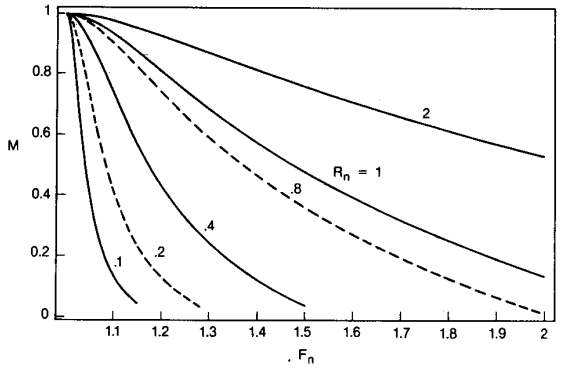

Fig. 9. Voltage gain versus normalized switching frequency for current-controlled switching.

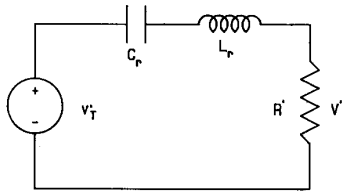

Fig. 10. Linear circuit to model the fundamental components of waveforms in a series resonant converter.

is restricted to a narrow band and switching loss is low over the entire load range with a mixture of current-controlled switching at heavy load and PWM at light load.

There are many possible control inputs which determine when to end the on interval that has been initiated when i_r crosses $\pm I_0$. A straightforward one is the on time itself: the on interval is terminated after t_1 seconds have elapsed. The control law from on time to voltage gain is derived from (10) and (14) and is plotted in Fig. 11. For better control of output current, the current-programming algorithms discussed in [6] may be used to terminate the on interval.

The normalized peak switch current is still described by (12). It is plotted against the voltage gain in Fig. 12. It varies almost linearly with the output voltage or, since each curve is for a constant load, load current. This is expected from the good form factor of the current waveform shown in Fig. 8(c).

In summary, the switch or inductor current in a series resonant converter can be sensed to determine when to switch with low loss. The range of frequency variation of the resulting switching scheme is narrower than that of a normal square-wave drive. The advantages of low switching stress and narrow-band frequency variation can be extended over the entire range of voltage gain or load by combining PWM with current-controlled switching.

IV. Experimental Results

A 100-W converter was built to verify analytical results. Its switching frequency was variable from 500 kHz down to 200 kHz, the resonant frequency. The input and

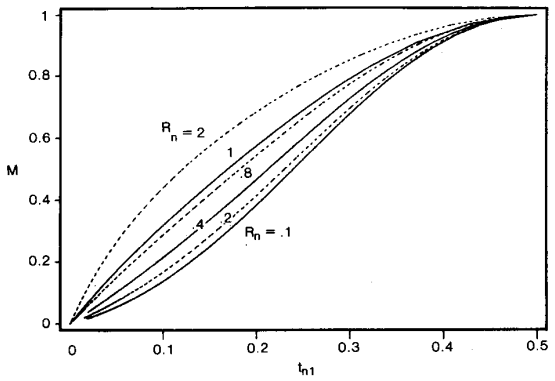

Fig. 11. Voltage gain versus normalized on time in current-controlled switching.

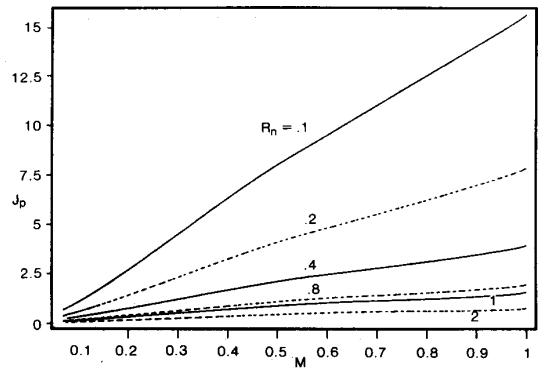

Fig. 12. Normalized peak switch current versus voltage gain in current-controlled switching.

output voltages were adjustable between zero and 50 V. In the PWM experiment, the components were as follows:

L_r	2.37 μH
C_r	0.263 μF
C	22 μF
R	15.3 Ω
Transistor	2SK399 (100 V, 10 A)
Rectifier	UES1301 (50 V, 6 A).

The passive components place the resonant frequency at 201.6 kHz and the normalized load resistance at 5.1. The drain-to-source voltage and current in one transistor are shown in Fig. 13(a) for $F_n = 1$, and in Fig. 13(b) for $F_n = 2$. Switching loss is low since the current is zero during turn-on and turn-off. There is some ringing on the voltage waveform due to the rapid discharging of the capacitance associated with the switched nodes.

Prediction and measurement of voltage gain as a function of duty ratio are compared in Fig. 14 for $F_n = 1$ and $F_n = 2$. The predicted gain is slightly higher than the measured one because it excludes circuit losses. The measured peak switch current agrees favorably with prediction. The efficiency ranged from 75 percent at low voltage gain to 90 percent at high voltage gain.

To verify the current-controlled switching functions, the

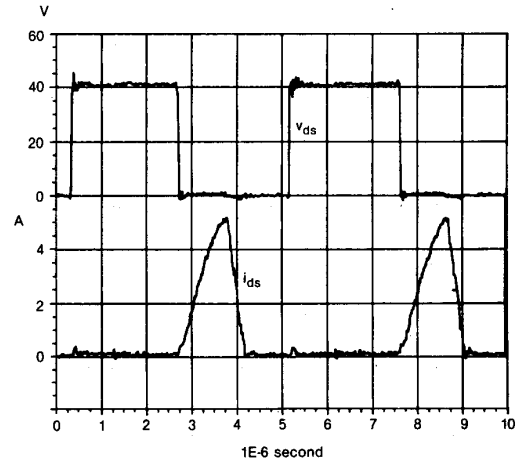

(a)

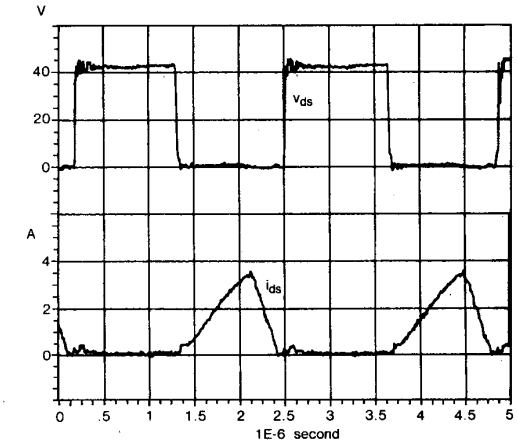

(b)

Fig. 13. Drain-to-source voltage (top trace) and current (bottom trace) for $F_n = 1$ (a) and for $F_n = 2$ (b). Output: 27 V.

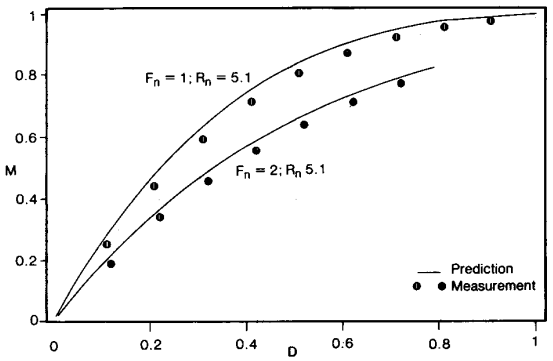

Fig. 14. Predicted and measured voltage gains versus duty ratio.

resonant components were modified as follows:

L_r	21.3 μH
C_r	29.5 nF.

These values leave the resonant frequency at 200.8 kHz and shift the normalized load resistance to 0.58. The

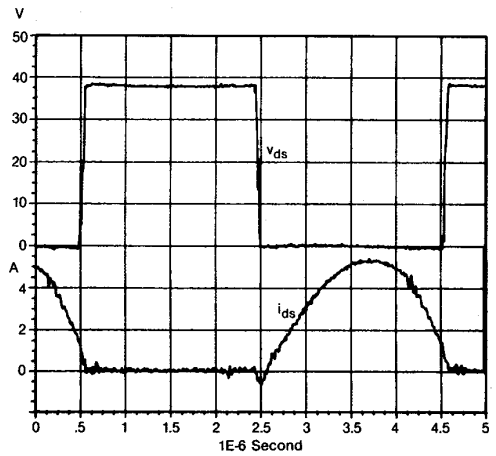

Fig. 15. Drain-to-source voltage (top trace) and current (bottom trace) for current-controlled switching. Output: 28 V.

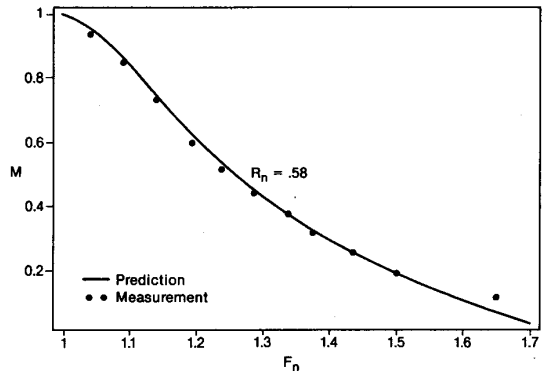

Fig. 16. Predicted and measured voltage gains versus normalized switching frequency for current-controlled switching.

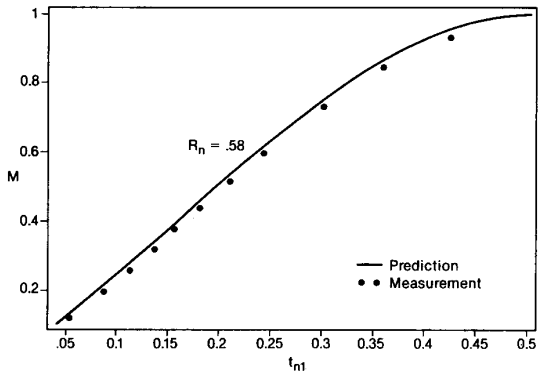

Fig. 17. Predicted and measured voltage gains versus normalized on time for current-controlled switching.

drain-to-source voltage and current are shown in Fig. 15. The switching period and on time were adjusted such that a small amount of current flowed through the inverse diode at turn-on. It is evident that the switching loss and noise are very low.

The range of frequency variation is confirmed in Fig. 16. The data for voltage gain as a function of normalized on time are compared in Fig. 17. Prediction and measurement agree well in general. The efficiency was between 75 and 90 percent from low voltage gain to high voltage gain.

V. Conclusion

For a full-bridge series resonant converter, pulsewidth modulation and current-controlled switching are viable drive alternatives that eliminate the difficulties faced by a simple square-wave drive. Both approaches apply phase-shifted drives to the full-bridge phase legs. When switching is above the resonant frequency, switching loss, noise, and stress are low. Therefore, these switching strategies are in harmony with the current trend of increasing the switching frequency into the megahertz range to improve the power density.

The main advantage of PWM is that the frequency does not have to vary since the duty ratio alone completely regulates the converter output for all line and load conditions. The benefit of low switching loss, however, is lost under heavy loading.

By using the switch or resonant inductor current to determine switching points, current-controlled switching offers very low switching loss and low circulating current for all loads. Even though the switching frequency needs to be varied, the range of variation is much narrower than that of a square-wave drive, especially at heavy load. Light-load regulation, however, requires a high upper frequency.

Since PWM is most beneficial at medium-to-light load while current-controlled switching is most advantageous at heavy-to-medium load, they should be combined so that their desirable characteristics are preserved over all loading conditions. Thus the resonant inductor current and current-control law determine switching instants under heavy and normal load, and PWM takes over under light load. Such a flexible switching scheme fully regulates the output, restricts the switching frequency to a narrow band, and commutates the switches smoothly (low loss, noise, and stress) under all line and load conditions.

Appendix

The equations describing a PWM full-bridge series resonant converter under discontinuous-conduction mode (dcm) are derived in this Appendix. One equation relates M to t_{n2} (the normalized quantity of t_2 in Fig. 2) and is used to determine the dcm boundary (Section II) and current-controlled switching gain (Section III). Another relates M to t_{n1} (the normalized t_1) and is used to determine the PWM gain (Section II) and current-controlled switching gain.

From Figs. 1 and 2, between 0 and t_1,

$$L_r \frac{di_r}{dt} = -v_r + V_g - V \tag{A1}$$

$$C_r \frac{dv_r}{dt} = i_r. \tag{A2}$$

The initial conditions for (A1) and (A2) are

$$i_r(0) = 0 \qquad v_r(0) = -V_0. \tag{A3}$$

The above equations are solved for I_1 and V_1, the values of i_r and v_r at t_1. The results are then normalized by (2) to give

$$J_1 = (M_0 - M + 1) \sin (2\pi t_{n1}) \tag{A4}$$

$$M_1 = 1 - M - (M_0 - M + 1) \cos (2\pi t_{n1}) \tag{A5}$$

where J_1, M_1, and M_0 are the normalized I_1, V_1, and V_0, respectively.

A similar procedure is used to find i_r and v_r at t_2. From Fig. 2,

$$i_r(t_2) = 0 \qquad v_r(t_2) = V_0. \tag{A6}$$

Therefore,

$$0 = J_1 \cos 2\pi(t_{n2} - t_{n1}) - (M_1 + M) \cdot \sin 2\pi(t_{n2} - t_{n1}) \tag{A7}$$

$$M_0 = (M_1 + M) \cos 2\pi(t_{n2} - t_{n1}) + J_1 \cdot \sin 2\pi(t_{n2} - t_{n1}) - M. \tag{A8}$$

Equations (A4) and (A5) are substituted for J_1 and M_1 in (A7) and (A8) to give

$$\sin 2\pi(t_{n2} - t_{n1}) = (M_0 - M + 1) \sin (2\pi t_{n2}) \tag{A9}$$

$$\cos 2\pi(t_{n2} - t_{n1}) = M + M_0 + (M_0 - M + 1) \cos (2\pi t_{n2}). \tag{A10}$$

The two preceding equations are squared, added, and solved for the following equation, important in determining the dcm boundary and current-controlled switching gain:

$$M = \frac{1 - \frac{M_0}{M} - \left(1 + \frac{M_0}{M}\right) \cos (2\pi t_{n2})}{1 + \left(\frac{M_0}{M}\right)^2 - \left[1 - \left(\frac{M_0}{M}\right)^2\right] \cos (2\pi t_{n2})}. \tag{A11}$$

The quantity M_0/M can be expressed in terms of the normalized load resistance R_n and the normalized switching frequency F_n. It can be seen from Fig. 1 that the load current is the average rectified i_r, which is proptional to the charge flowing through C_r from 0 to t_2:

$$\frac{V}{R} = \frac{2}{T} \int_0^{t_2} i_r \, dt = \frac{4}{T} C_r V_0. \tag{A12}$$

Upon normalization (A12) becomes

$$\frac{M_0}{M} = \frac{\pi}{2R_n F_n}. \tag{A13}$$

The relationship between M and t_{n1} is derived by equating the input energy to the output energy. Over each half cycle,

$$E_i = V_g \int_0^{t_1} i_r \, dt = E_0 = V \int_0^{t_2} i_r \, dt. \tag{A14}$$

Note that the integrations represent the charges flowing through C_r and, hence, the changes in v_r over the specified integral limits. The changes in v_r are computed from (A3) and (A5) and substituted for the integrations in (A14) to give

$$\cos (2\pi t_{n1}) = 1 - \frac{2M}{1 + \frac{2R_n F_n}{\pi}\left(\frac{1}{M} - 1\right)}. \tag{A15}$$

This equation is used in calculating both PWM and current-controlled switching gains.

References

[1] V. Vorperian and S. Cuk, "A complete dc analysis of the series resonant converter," in *IEEE Power Electronics Specialists Conf. 1982 Rec.*, pp. 85-100.

[2] R. L. Steigerwald, "A comparison of half-bridge resonant converter topologies," in *IEEE Applied Power Electronics Conf., 1987 Proc.*, pp. 135-144.

[3] F. C. Schwarz, "An improved method of resonant current pulse modulation for power converters," in *IEEE Power Electronics Specialists Conf. 1975 Rec.*, pp. 194-204.

[4] A. F. Witulski and R. W. Erickson, "Steady-state analysis of the series resonant converter," *IEEE Trans. Aerosp. Electron. Syst.*, vol. AES-21, no. 6, pp. 791-799, Nov. 1985.

[5] F. G. Turnbull and R. E. Tompkins, "Design of a pulsewidth modulated resonant converter for a high output voltage power supply," in *IEEE Industry Applications Society Annu. Meet. 1985 Rec.*, pp. 1145-1150.

[6] V. Nguyen and J. Dhyanchand, "An implementation of current-mode control for a series-resonant dc-dc converter," in *IEEE Applied Power Electronics Conf. 1987 Proc.*, pp. 266-273.

[7] R. P. Severns and G. E. Bloom, *Modern DC-to-DC Switchmode Power Converter Circuits*. New York, NY: Van Nostrand-Reinhold, 1985.

[8] C. W. Deisch, "Simple switching control method changes power converter into a current source," in *IEEE Power Electronics Specialists Conf. 1978 Rec.*, pp. 300-306.

Khai D. T. Ngo (S'82-M'84) received the B.S. degree in electrical and electronics engineering from California State Polytechnic University, Pomona, in 1979, and the M.S. and Ph.D. degrees in the same discipline from the California Institute of Technology, Pasadena, in 1980 and 1984, respectively.

He has been a Member of Technical Staff at GE Corporate Research and Development Center, Schenectady, NY, since July 1984. His research interests are in ac converter topology and control, high-frequency converters and components, power integrated circuits, and computer-aided design for power electronics. He has published seven papers.

Dr. Ngo is a member of Phi Kappa Phi, Tau Beta Pi, Eta Kappa Nu, and Sigma Xi.